This article has been accepted for inclusion in a future issue of this journal. Content is final as presented, with the exception of pagination.

Simple Method to Extract Lake Ice Condition From Landsat Images

Xiao Yang, Tamlin M. Pavelsky, Liam P. Bendezu, and Shuai Zhang

***Abstract*— Ice plays key roles in regulating hydrological, ecological, biogeochemical, and socioeconomic functions of lakes. Long-term *in situ* lake ice phenological records indicate that lake ice is trending toward later freeze-up, earlier breakup, and a shorter ice duration. Parallel to study of lake ice using *in situ* records and process-based models, satellite remote sensing can expand our understanding of lake ice change over large spatial scales. However, most remote sensing studies have focused on large lakes or short periods of time, which may not robustly represent changes over multidecadal time periods or in the much more numerous small lakes. Here, we present a random forest model, Sensitive Lake Ice Detection (SLIDE), to accurately extract ice conditions from Landsat TM, ETM+, and OLI images. We trained the model using a manually labeled lake ice dataset (1089 labeled areas over 995 lakes globally). Our results show that our model achieves accurate classification between ice/snow and water (accuracy: 97.8%, kappa coefficient: 95.5%). Comparing Landsat-derived ice cover with *in situ* ice conditions, we show that our model produces less bias, lower RMSE, and higher kappa than does the Landsat snow/ice flag from the quality assessment band. This is especially true during the transitional period surrounding the ice on and off dates reported from *in situ* (mean bias −7.3% from our model, −17.3% from the Landsat quality band). Our results demonstrate the feasibility of mining the rich Landsat archive to study lake ice dynamics and of better flagging ice-affected lake observations.**

***Index Terms*— Lake ice, Landsat, random forest.**

I. Introduction

MOST of the world's lakes formed in post-glacial landscapes [1], so they tend to be in cold regions that promote the development of seasonal ice cover. Because lakes are located at local topographic lows, they collect the detritus of their surrounding landscape and act as hot spots for many biogeochemical, ecological, and nutrient processes [2]–[4]. For lakes located in the cold regions, seasonal ice cover regulates many aspects of lake functions [5], [6]. For example, ice cover can reduce annual evaporation from lakes, which is expected to increase by 16% globally by the end of the 21st century, partly due to shortening ice duration [7]. Lake ice also provides niches for under-ice ecosystems to develop and endure through winter [8], [9]. A recent study demonstrated various ways in which loss of river and lake ice could reduce cultural ecosystem services [10]. Lake ice has also been shown as an important regulator to the flux of CO_2 and methane, with field data showing their release at ice-melt period accounting for 17% and 27% of the annual emission [2]. Due to the high prevalence of lake ice and the tight integration of ice cover with lakes' functions, it is important for us to understand the spatiotemporal distribution of seasonal ice cover in lakes and how they respond to ongoing warming. Indeed, existing studies based on *in situ* data have already found widespread shortening of lake ice duration, resulting from later freeze-up or earlier breakup of ice or both [11]–[13], and that such trends can be detrimental to hydrological, ecological, biogeochemical, and cultural functions.

Equally important is our ability to flag ice-affected areas from remote sensing images. Landsat images have been widely used to develop lake water quality retrieval algorithms [14], [15]. Existing studies using Landsat for lake water extent and quality monitoring either used the snow/ice quality flag [16], [17], applied prior knowledge of the ice-free months [18], [19], or visually inspected each instance [20] to remove influence of ice cover. As remote sensing of inland water quality moves from focusing on method development to application [15], it is critical for us to be able to flag the influence from ice accurately and efficiently.

Long-term monitoring of lake ice generally relies on *in situ* observation, with the longest records spanning centuries [11]. *In situ* records have been widely used to study lake ice phenology trends and to predict future lake ice conditions [21]. However, lakes with *in situ* records are limited both in number and in spatial coverage. For example, while the global lake and river ice phenology dataset (GLRIP) [22], which aims to aggregate globally lake ice phenology from historical records, includes 631 lakes, this number is still far fewer than the 1.4 million lakes registered in the HydroLAKES dataset [23]. Moreover, lakes with *in situ* records tend to be located in the Northern Hemisphere, concentrated in a few lake-rich and relatively developed countries, and lacking spatial coverage over the global south and other lake-rich regions like the Tibetan Plateau or Siberia.

Manuscript received September 17, 2020; revised April 28, 2021; accepted May 30, 2021. This work was supported in part by the SWOT Project Office through a subcontract at the National Aeronautics and Space Administration (NASA)/Caltech Jet Propulsion Lab and in part by the NSF Navigating the New Arctic (PI: A. Lynch, Brown U.) under Grant #2022554. *(Corresponding author: Xiao Yang.)*

Xiao Yang, Tamlin M. Pavelsky, and Liam P. Bendezu are with the Department of Geological Sciences, University of North Carolina at Chapel Hill, Chapel Hill, NC 27599 USA (e-mail: yangxiao@live.unc.edu; pavelsky@email.unc.edu; lbendezu@live.unc.edu).

Shuai Zhang was with the Department of Geological Sciences, University of North Carolina at Chapel Hill, Chapel Hill, NC 27599 USA. He is now with the College of Marine Science, University of South Florida, St. Petersburg, FL 33701 USA (e-mail: tamuzhang@gmail.com).

This article has supplementary downloadable material available at https://doi.org/10.1109/TGRS.2021.3088144, provided by the authors.

Digital Object Identifier 10.1109/TGRS.2021.3088144

In contrast to *in situ* measurements, optical remote sensing has been used to estimate ice phenology for many lakes and rivers worldwide [24], [25]. Because lake ice often (though not always) appears bright with higher reflectance values at visible and near-infrared wavelengths, while open water appears dark, optical sensors are an appealing option for measuring lake ice extent. Given its ability to provide daily global images, the Moderate Resolution Imaging Spectroradiometer (MODIS) has been perhaps the most commonly used to estimate lake ice phenology [26], [27]. Using MODIS, a recent study by Šmejkalová [24] estimated trends in lake ice breakup timing for key regions across the pan-Arctic.

Unfortunately, moderate resolution optical sensors like MODIS have relatively coarse resolution compared with sizes of lakes that are most abundant and also suffer from having a relatively short period of observation, starting in 2000, that prevents clear separation between long-term trends and interannual variability. Due to both clouds and poor sunlit surface during the period that freeze-up takes place, estimating lake ice freeze-up from MODIS remains a challenge. Compared with MODIS, Landsat TM, ETM+, and OLI imagers have a much higher spatial resolution (30 m, instead of highest resolution of 250 m for MODIS) that makes direct observations of smaller lakes possible. This higher spatial resolution also facilitates observations during the freeze-up period. While its 16-day repeat does not allow phenology estimation on a year-by-year base, aggregating records temporally can reveal climatological ice duration and its long-term change [25]. Because Landsat TM data are available beginning in 1984, a >36 year data record is now available for much of the globe. This longer record can facilitate measurement of patterns and trends in ice breakup date, freeze-up date, and duration.

Each Landsat TM, ETM+, or OLI image has a quality flag indicating whether a pixel is affected by snow/ice. The algorithm used to classify snow/ice was derived based on the MODIS snow algorithm and detailed in [28]. However, performance of this snow/ice classification has not been systematically evaluated, in particular for identifying lake ice. Only one study has considered Landsat to map lake ice conditions. By using Landsat OLI images, Barbieux *et al.* [29] developed a tree-based classification method that can differentiate dark ice, opaque ice, and water pixels over a lake surface. Although focused on only a few lakes, it demonstrated the feasibility of using Landsat to study lake ice. Meanwhile, Yang *et al.* [25] assessed the per-pixel snow/ice quality flag stored in the quality assessment band of Landsat images over rivers and found that it can accurately distinguish water and snow/ice except that it tends to misclassify water with high sediment as snow/ice and to miss dark ice (where optically thin ice allows signal from water and ice to mix). This dark ice is notably more common over lakes than rivers due to lakes' less dynamic environment compared with the latter.

The goal of this article is to describe and evaluate a globally applicable method to accurately identify the presence or absence of lake ice using Landsat imagery. Because we are unaware of any current database of lake ice conditions, we manually labeled lake surfaces in over 1000 Landsat images into areas of "Water," "Dark ice," and "Opaque ice/Snow." Then, we developed a random forest model [30] named Sensitive Lake Ice Detection (SLIDE), leveraging both spectral and texture properties extracted from random subsets of pixels in the labeled lake areas. We evaluated our model against manually labeled data and against the *in situ* lake ice phenology dataset.

II. Method

A. Developing Training Dataset

1) Selecting Landsat Images for Manual Labeling: Humans are good at identifying objects based on their patterns and spatial and temporal context, thus, many machine learning image analysis algorithms either directly incorporate expert knowledge during development [31] or are trained on the data labeled by humans. To select the optimal sets of lakes and images to manually label different lake surface conditions, we combined two different strategies: 1) selection based on magnitude of surface air temperatures; and 2) selection based on both surface air temperature and the ice fraction estimated from the Landsat quality assessment band (which was calculated based on Fmask [28]).

To apply these two strategies, we first built a preliminary global lake ice dataset. We calculated lake ice fraction, cloud cover fraction, and 30-day prior surface air temperature for all lakes with size ≥ 1 km^2. The extents of lakes were based on the HydroLAKES dataset [23], with both the lake ice fraction and cloud cover fraction estimated based on the Fmask-derived snow/ice and cloud/shadow flags, respectively. The mean surface air temperature was estimated based on daily 2-m air temperature from the ERA5 climate reanalysis data [Copernicus Climate Change Service (C3S) (2017)]. After building the dataset, records were removed from the dataset if cloud cover exceeded 10%. This resulting global Fmask-derived lake ice dataset was used to help select the optimal lake-image pairs for our manual labeling process.

To select lake-image pairs that diversify air temperature, we sampled the lake-image pairs stratified by 30-day prior mean surface air temperature (SAT). Specifically, we binned the mean SAT into ten equal intervals from -49 °C to 43 °C (determined by the actual SAT range experienced by lakes); then, from each group, we randomly sampled up to 100 lake-image pairs (we included all samples for groups having less than 100 records). Collecting training data from across a wide SAT range allows the training data to provide information on characteristics of ice cover and open water on lakes, both of which are critical for accurate detection of ice cover. Similarly, to select lake-image pairs based on both temperature- and Fmask-derived ice fraction, we intentionally selected images capturing the transitional period between open water and ice to explore potentially challenging cases for Fmask-based snow/ice classification [25]. We assumed that lake ice coverage between 15% and 85% likely indicated partial ice cover; thus, we repeated a similar stratified-sampling approach using the mean SAT temperature binning but limited to only sample the records with Fmask-derived ice fraction within the 15%–85% range. Combining lake-image pairs from both subsets, we obtained 995 lake-image pairs (350 of which

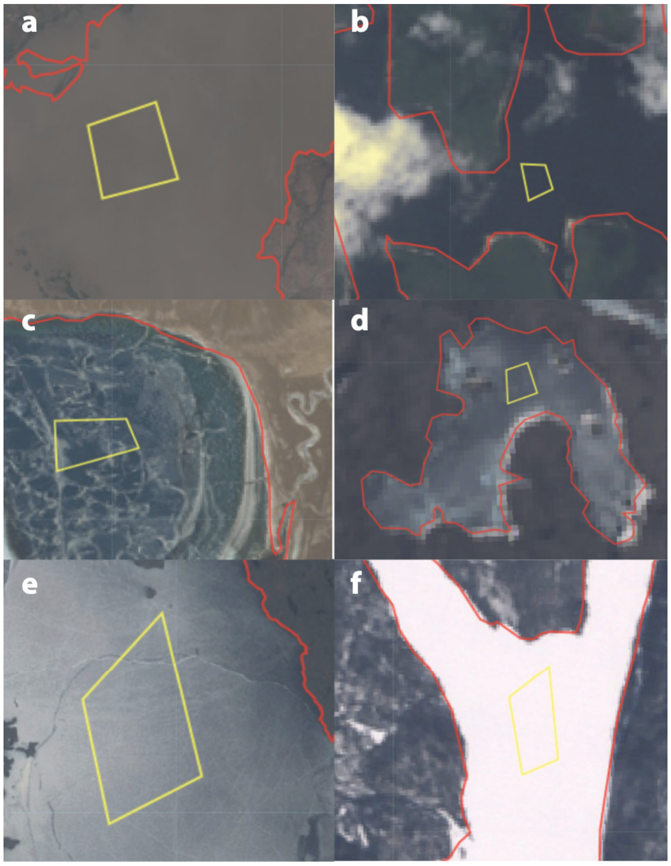

Fig. 1. Examples of manually labeled lake surface types. (a) and (b) Water, (c) and (d) dark ice, and (e) and (f) snow/opaque ice. Yellow polygons are manually labeled regions and red lines are the lake boundary from HydroLAKES database.

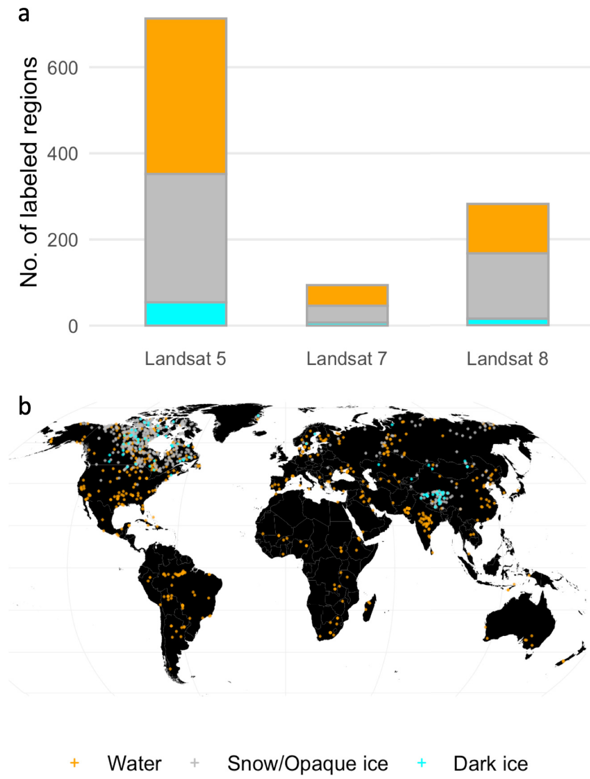

Fig. 2. Characteristics of the labeled dataset. (a) Number of labeled polygons for Landsat sensors colored by contribution from each type. Note that the proportion of images from different satellites scale with the years of observation used (Landsat TM: 1984–2013, Landsat ETM+: 1999–2003, Landsat OLI: 2014–2018). (b) Map shows locations of labeled polygons used to generate training data, with color to differentiate different types of lake surface.

showed partial ice cover) in total to serve as the source of the training dataset.

2) Manually Labeling Lake Areas Via Visual Inspection: We established a workflow to visually identify lake ice conditions in the Google Earth Engine platform [32]. For each lake-image pair, we manually drew polygon region(s) within the lake surface defined by HydroLAKES that belong to one of the three classes ("Water," "Dark ice," and "Opaque ice/Snow"). For the majority of the time, the difference among the three classes was distinguishable and clear from the "Red-Green-Blue" (or RGB) band combination, so we only had to look at the RGB image. However, there were times that we refer to a modified normalized difference water index (MNDWI) [33] layer to assist identification of the land–water boundary.

We used the following criteria to classify lake surface conditions. If a region of the lake surface was dark and uniform without any bright irregular linear structures, then we classified it as "Water"; if a region of the lake was somewhat brighter with irregular linear structure across its surface, then we classified it as "Dark ice"; and if a region of the lake appeared very bright, then we labeled it as "Opaque ice/Snow" (see examples in Fig. 1). It is worth noting that we did not include a class for cloud, as we used the cloud shadow and cloud flag provided in the quality assessment band [28]. During the labeling process, we specifically tried to avoid labeling regions that overlapped with any visually discernible cloud cover. Afterward, when we prepared the data for model development, we removed all data detected by Fmask as cloud or cloud shadow.

In total, we manually labeled 1,089 regions in lakes that distributed across the globe (Fig. 2). The distribution of regions across different satellite images reflects proportionally the availability of data. For Landsat ETM+, we only used images captured before the malfunction of its Scan Line Corrector in May 2003.

3) Extracting and Cleaning the Labeled Dataset: For each training area that we manually drew in the previous step, we randomly sampled 50 distinct pixel (or all the pixels if the region contains fewer than 50 pixels). For each pixel, we extracted relevant spectral and texture information. Spectral variables included the top of the atmosphere reflectance (TOA) values for the following bands: "Red," "Green," "Blue," and Near-infrared ("Nir"). The texture variable was the average gradient of the "Blue" band in a 5 pixel $\times$ 5 pixel kernel, adapted from Barbieux *et al.* [29], who found the average gradient of the "ultra Blue" band to be an important variable in identifying lake ice. In addition, we extracted variables required as input to the model of water sediment content and several water color metrics (see Table I). Specifically, we used the green/blue ratio, the red/green ratio, and the normalized

TABLE I
PREDICTORS USED FOR TRAINING SLIDE

Predictor name	Values range	Notes
Nir	0–1	[29]
WICI	n/a	WICI: Water-Ice classification index [29]
gBlue	positive	Gradient of the Blue band, adapted from Barbieux et al. [29]
Green	0–1	Fmask snow/ice algorithm [28]
hue	0–1	Color metric
saturation	0–1	Color metric
value	0–1	Color metric. Represent the brightness of the color
NDSSI	-1–1	Normalized Difference Suspended Sediment Index from Hossain et al. [34]
Green/Blue	positive	Band ratio
Red/Green	positive	Band ratio
Landsat	[5, 7, 8]	Categorical variable indicating Landsat mission

difference suspended sediment index (NDSSI) using the Blue band and Nir band to provide relevant information about water column constituents. We also used water color, converted from red, green, and blue band reflectances and represented by hue, saturation, and value (i.e. brightness), to inform the model about ice cover conditions. Finally, we extracted the quality flag for each pixel location to help remove cloud-affected records and to compare the Fmask snow/ice flag with our new model. Specifically, we extracted the flags for "Cloud," "Cloud shadow," and "Snow/ice" from the quality assessment band. In total, we obtained 51 167 labeled records from 995 lakes over 973 unique Landsat TOA images.

B. Developing a Random Forest Lake Ice Model

While many machine learning methods are available for classification, we chose random forest because it generally outperforms single-tree approaches while still sharing the advantages of tree-based methods, which can be effective in detecting lake ice [29]. We developed the model directly in Google Earth Engine to allow rapid application for future studies. We recognize the potential to improve upon our random forest method via other machine learning methods, especially those used in computer vision (e.g., convolutional neural networks, deep learning, etc.). To facilitate future development of machine learning lake ice algorithms, we make public the raw polygons and their corresponding Landsat image ID (see Data and Code).

TABLE II
RANGES AND INTERVALS USED TO TUNE PARAMETERS FOR THE RANDOM FOREST MODEL

Parameter name	Minimum value	Maximum value	Increment
ntree	150	350	100
nsplit	2	8	1
nmaxnode	15	48	3

Three variables parameterize a random forest classification: 1) ntree: number of trees generated in the random forest; 2) nsplit: number of predictors randomly selected to train each individual tree; and 3) maximum number of leaf nodes allow for each tree construction. To identify the optimal model parameterization, we tuned the parameters of the random forest model using the following approach: We iteratively divided all the lakes in the dataset into a training set (70%, $N_{\text{lake}} = 710$) and a testing set (30%, $N_{\text{lake}} = 285$). We then developed a random forest model with each possible combination of the tunable parameter values given in Table II. Then, we repeated the process ten times to reduce the randomness from splitting lakes into training and testing sets. For each of the 2520 random forest models constructed, we calculated and recorded values of accuracy (q) and kappa coefficient (k) [35]. The recorded classification helps us determine the optimum set of parameters.

It is worth noting that we chose to use the lakes as the base unit to split the labeled records into training and testing/validation sets. This approach reduces the potential for overfitting when different polygons from the same lake are used to train and test the model [36].

C. Evaluating Model Performance

1) Evaluating Model Performance at the Pixel Level: After identifying the optimal model parameterizations, we calculated the accuracy and kappa coefficients for the final model prediction based on data from the 30% of lakes that were kept for validation ($N_{\text{record}} = 14\,407$, $N_{\text{lake}} = 285$). We also estimated the same metrics for the snow/ice flag from the Landsat quality band.

2) Estimating Lake Ice Fraction and Compared With In Situ Records: To evaluate our model at lake scale against *in situ* ice phenology data, we compared Landsat-derived ice coverage from both the SLIDE and the Fmask to *in situ* records from Alaska [37], [38] and from the global lakes and rivers ice phenology (GLRIP) dataset [22].

Lake ice phenology for Alaskan lakes was obtained from literature [37], [38] and only those with both freeze-up and breakup dates were used. The phenology was determined based on either *in situ* observations or remote sensing images. And the data contained lake location (in pairs of longitude and latitude) and dates for ice breakup and freeze-ups. The GLRIP dataset contains similar information on annual ice phenology, lake name, and lake location (as longitude and latitude values).

Both GLRIP and Alaskan lakes need to be matched with their spatial extent, before the Landsat-derived ice coverage can be calculated and compared with the *in situ* ice conditions. To do this, we spatially and temporally matched Landsat-derived ice fraction to *in situ* records. Spatially, we paired lakes (given as point locations) in GLRIP and from Alaska to the polygons of lake boundaries from HydroLAKES. Note that point locations given in the GLRIP phenology dataset came from various data contributors and have different accuracies and precisions. Instead of using locations from the original phenology dataset, we used updated lake locations developed by Sharma *et al.* [21]. We also manually checked and updated when necessary all the lake locations based on lake names registered in the GLRIP dataset. After updating locations, we were able to confidently match 287 of the 327 lakes in the GLRIP dataset, and 50 of the 57 Alaskan lakes that have valid records from 1984 and onward to lake polygons in HydroLAKES. To increase the potential temporal matches between the Landsat-derived and *in situ* data, we assumed that, for a given lake in the *in situ* lake datasets, the lake surface was fully ice covered (i.e. ice fraction = 100%) between the date of freeze-up and the breakup date in the following calendar year; similarly, we assumed the lake surface was fully ice free (i.e. ice fraction = 0%) between the date of breakup and the following freeze-up in the same calendar year. After matching satellite and *in situ* datasets for individual years, we then excluded paired records that exceeded 10% cloud cover. In the end, we obtained 17,339 ($n = 17\,323$ from GLRIP and $n = 16$ from Alaskan dataset) paired annual records over 226 lakes (220 from GLRIP and 6 from Alaska) that we used to evaluate the SLIDE and the Fmask snow/ice flag (Fig. 3). Note that distribution of the *in situ* data was largely limited to locations at lower latitudes where historical records were relatively abundant. Publicly available lake ice phenology data are unfortunately scarce in lake-rich regions of Alaska, Siberia, and northern Canada.

We used two sets of metrics to compare Landsat-derived lake ice fraction (0%–100%) to the *in situ* ice condition (ice-cover or ice-free). To estimate error metrics suitable for continuous data, such as RMSE (root mean square error), MAE (mean absolute error), and MBS (mean bias), we converted the *in situ* ice phenology dates into ice fraction of 0% (when ice-free) and 100% (when ice-cover). Conversely, to estimate classification accuracy that is based on categorical data, we converted the continuous ice fraction from Landsat (both Fmask and SLIDE) to binary ice conditions with a fixed threshold (50%) so that the lake is ice covered when ice fraction $\geq$50%, and ice-free otherwise. We estimated these metrics both using the entire matchup dataset and using only the data from the transition periods, which are defined as the dates that are $\leq$15 days away from any given ice-on or ice-off dates in the *in situ* dataset. The transition periods usually represent the most dynamic period of time for lake ice formation and breakup. As a result, they are also a challenging time to accurately estimate ice cover fraction, thus providing a good worst case scenario to evaluate model performance.

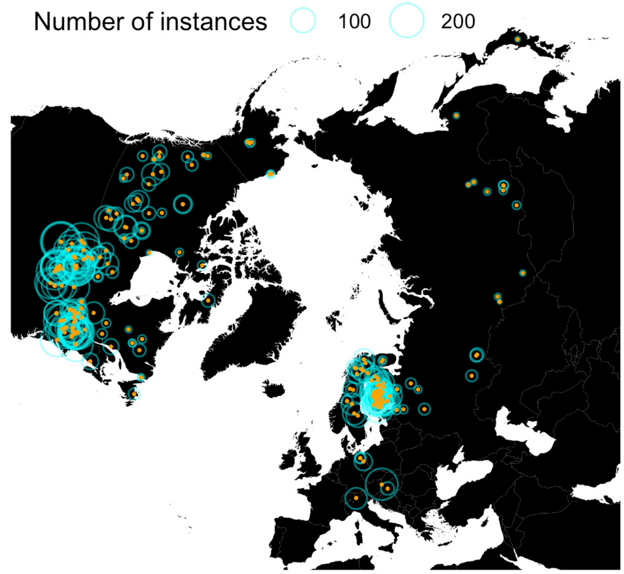

Fig. 3. Distributions of paired, cloud-free, Landsat-derived and *in situ* ice records. Orange point locations denote lake used and size of the cyan circle denotes the number of matching instances between Landsat-derived ice records and lake ice condition derived from the *in situ* records.

3) Visually Comparing With Satellite Images: The aforementioned evaluation methods are based on summary statistics and do not necessarily accurately reflect how predicted lake surface condition matches with true ice cover spatially within a particular lake. In order to evaluate spatial patterns of ice cover within lakes and their accuracy, we mapped lake ice conditions as predicted by our algorithm and compared them visually against Landsat RGB composite of the lake. While we would ideally like to conduct this type of validation automatically, we are not aware of any way to do so. Specifically, we selected a total of 100 randomly chosen records from the 2760 transitional matchup records with *in situ* data where the *in situ* lake ice condition was substantially different from the ice fraction estimated by SLIDE: ice fraction $\leq$50% when *in situ* suggests ice cover, or ice fraction $\geq$50% when *in situ* suggests ice free. These records were divided equally between ice free and ice cover conditions (inferred from *in situ* phenological dates) and limited only to the transitional periods.

III. RESULTS

A. Parameter Tuning and SLIDE

We selected the final set of values for model parameters using the following criteria: 1) we maximized the accuracy and kappa coefficients calculated from the testing data; 2) we minimized the commission error for ice calculated from the testing data; and 3) in the absence of substantial improvements in accuracy, kappa, and commission error, we preferred a simpler model (e.g., fewer trees, smaller nsplit, and nmaxnode) over a complex one. Based on these criteria, we set the final

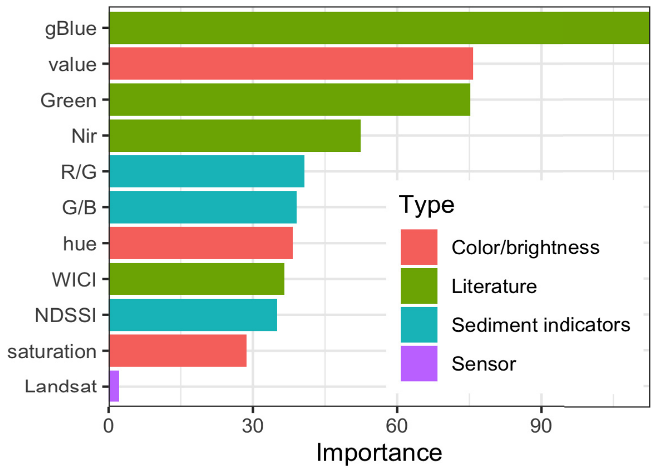

Fig. 4. Variable importance from SLIDE.

model parameter values as follows: ntrees = 250, nsplit = 2, nmaxnode = 24. This set of parameters values yielded $q = 97.1 \pm 0.7\%$, $k = 94.2 \pm 1.4\%$, and mean commission error of ice = 1.7% when compared against testing data (values presented in "mean ± stand deviation" format).

We randomly selected 70% of the lakes ($N_{\text{record}} = 36\,760$, $N_{\text{lake}} = 710$) in the labeled dataset to train the final random forest model; the remaining data ($N_{\text{record}} = 14\,407$, $N_{\text{lake}} = 285$) were used to derive the final model error metrics. Variable importance from SLIDE (Fig. 4) confirmed that predictors used in previously published algorithms (e.g., gBlue, Green, Nir) for ice and snow detection are highly effective. It also demonstrated the importance of variables not included in previous models, as indexes for water color (hue, saturation), brightness (value), and sediment can help substantially in differentiating ice from water. In contrast, the indicator of Landsat sensor is the least important variable tested, suggesting only minor compensation is needed for the algorithm to work across sensors.

B. Model Evaluation

1) Pixel-Level Evaluation: Validating against the labeled data from the 30% holdout lakes ($N = 285$), SLIDE was able to predict $q = 97.8\%$ ($k = 95.5\%$) of the 14 407 cases in the validation data. We also compared the Landsat's Fmask-based snow/ice flag for these pixels to our manually labeled class and found that its accuracy fell short compared with SLIDE, with $q = 89.3\%$ and $k = 78.2\%$.

2) Evaluation Against In Situ Records: Comparing both the Fmask- and SLIDE-derived ice fraction with *in situ* records, we found that SLIDE had higher accuracy and kappa coefficient compared with that estimated from Fmask, though both were quite accurate, having $q \geq 95\%$. RMSE, MAE, and MBS for both methods are similar, though SLIDE consistently showed smaller error terms and biases compared with Fmask (Table III). This high accuracy is not unexpected, as, in many cases, the presence or absence of ice is unambiguous. The disparity in accuracy and error metrics is much greater during the crucial transition period surrounding ice freeze-up and

TABLE III

MODEL PERFORMANCE EVALUATED AGAINST *In Situ* DERIVED LAKE SURFACE CONDITION

Entire dataset					
Model	**RMSE**	**MBS**	**MAE**	**Accuracy**	**Kappa**
SLIDE	15.3%	-1.0%	3.5%	97.1%	93.5%
Fmask	19.0%	-3.4%	4.7%	95.6%	89.9%
Transitional period					
Model	**RMSE**	**MBS**	**MAE**	**Accuracy**	**Kappa**
SLIDE	33.3%	-7.3%	15.8%	86.2%	72.3%
Fmask	42.2%	-17.3%	22.1%	78.4%	56.7%

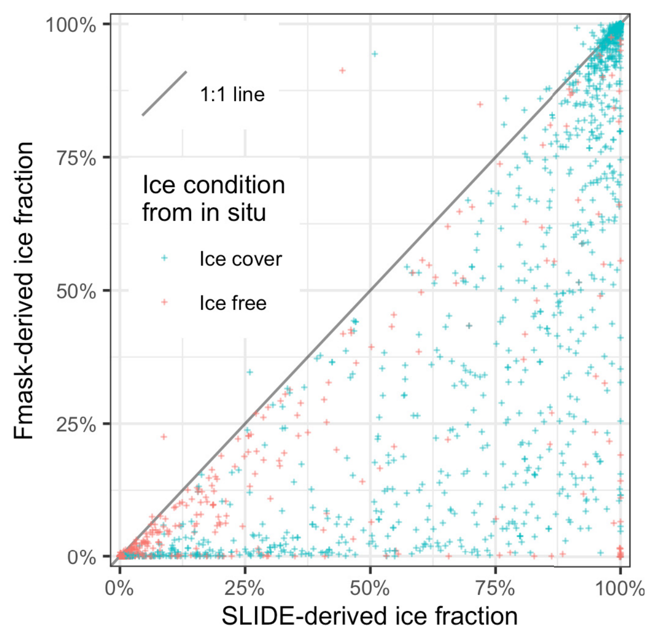

Fig. 5. Comparison between *in situ*, SLIDE-derived, and Fmask-derived lake ice cover for the matchup records that fall within the transition period ($N = 2760$). Note that the ice conditions denoted by color were derived from *in situ* lake ice phenology to facilitate comparison between remotely sensed ice fraction and *in situ* lake ice condition.

breakup. For example, MBS for SLIDE is less than half of that for Fmask during transition period, and accuracy and kappa coefficients are substantially higher for SLIDE ($q = 86.2\%$, $k = 72.3\%$) than for Fmask ($q = 78.4\%$, $k = 56.7\%$).

Comparing lake ice fraction estimates from SLIDE with those from Fmask for lakes having *in situ* lake ice data, we found that SLIDE almost always predicted higher ice cover fraction (Fig. 5), due to the improved ability of SLIDE to detect dark ice. We also observed that SLIDE seemed to occasionally misclassify water and ice, for example, estimating low ice fraction for *in situ* data suggested ice cover (Fig. 5). However, as we demonstrate in the next section, it is likely

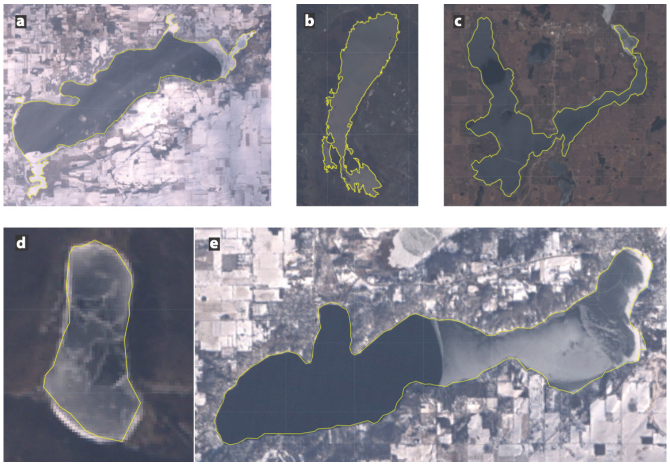

Fig. 6. RGB Landsat images showing example cases encountered when manually evaluating SLIDE-derived ice cover. (a) Example of commission error when SLIDE misclassified open water as ice due to thin cloud cover (id = 9039). (b) Example of commission error when turbid water was misclassified as ice (id = 1242). (c) Example of omission error where SLIDE misclassified thin ice cover as water (id = 9069). (d) Example showing when the texture of ice presents, SLIDE can accurately classify ice (id = 110973). (e) Example showing challenges arise when comparing satellite-based measurement with that from *in situ* due to difference in viewing aspect (id = 9110). Note: lake locations identified by their id in HydroLAKES database.

that many of these apparent errors represent a failure in the assumption we used to convert *in situ* phenological dates into ice fractions rather than in SLIDE itself.

3) Visual Evaluation: We examined 100 cases of Landsat lake surface images collected during the transitional period to visually estimate the extent of lake ice cover and assessed how it compared with the spatial extent of SLIDE snow/ice classification. In 22 cases, lake surface conditions cannot be clearly determined (11 due to cloud cover, 10 were unclear due to small lake surface area, 1 was due to the image not fully covering the lake surface). Of the remaining 78 valid cases, we observed 8 cases of commission error (10.3%) and 30 cases of omission error (38.5%) of SLIDE-predicted snow/ice cover compared with our visually determined ice extent. In the remaining 40 cases (51.3%), SLIDE accurately matched the visually determined lake ice extent. As described in the Methods section, we selected these records based on the criterion that the SLIDE-derived ice fraction was inconsistent with the *in situ* ice condition. Our visual evaluation thus suggests that approximately half of the cases identified as errors based on a simple statistical comparison with *in situ* data are, in fact, correctly classified by SLIDE.

Five of the eight cases of commission error were caused by misclassifying clouds as snow/ice [Fig. 6(a)], and the rest were caused by poor image quality (triggered the texture variable to identify snow/ice, two cases) and turbid water [one case, see Fig. 6(b)]. Of the 30 cases of omission error, five featured opaque ice misclassified as water by SLIDE, probably due to the smooth texture of the ice surface [see Fig. 6(c)]. The remaining 25 cases were all caused by SLIDE not being able to detect varying degrees of dark ice. However, across all cases where dark ice was present, SLIDE detected ice more successfully than Fmask [e.g., Fig. 6(d)]. We also noticed, not infrequently, that images seem to suggest ice conditions contrary to those derived from *in situ* [see, e.g., Fig. 6(e)]. This contradiction is mainly caused by the fact that during the transitional period, using an observed freeze-up or breakup date to identify a binary lake condition (ice-covered/ice-free) does not allow for the complexity of partially ice covered lakes.

For each of the 78 valid cases, we visually estimated ice fraction into five intensity categories with a 20% increment. For example, category 1 means ice fraction lies between 0 and 20% and category 5 means ice fraction lies between 80% and 100%. Based on these ice fraction estimates, we found that only 45% of cases were in category 5 when *in situ* suggested ice cover; and when *in situ* suggested ice free, only 15% of cases were placed in category 1, a proportion even smaller than the cases in category 5, which had 42% of the cases. Other potential reasons for differences between the visually determined ice fraction and the ice condition based on *in situ* records are: 1) some lakes undergo multiple freeze-thaw events, so a single phenological date will not accurately set the boundary for ice cover and ice free conditions; 2) an *in situ* observer sees only a portion of larger lakes from a point on the ground, while remote sensing methods observe the entirety of the lake described by HydroLAKES; and 3) boundaries of the lakes observed *in situ* and defined by HydroLAKES may be different, especially for lakes with highly complex geometrical shape or those bearing multiple names (e.g., many connected water bodies in Finland share one identity in the HydroLAKES database but each has its own name that is used in the *in situ* dataset). As such, in some cases, we believe that apparent errors of both commission and omission relative to *in situ* data may, in fact, simply reflect the different observing capabilities of remote sensing and *in situ* methods.

IV. Discussion

In this study, we developed a lake ice classification model based on random forest that can be applied to satellite images from Landsat TM, ETM+, and OLI. By strategically selecting images reflecting variable conditions for lakes across the globe to develop our training data, and by using a data-driven approach to optimize the lake ice classification algorithm, the lake ice model presented in this study shows substantial improvement in accuracy compared with the existing snow/ice flag based on Fmask. It is also more broadly applicable and more accurate than the model developed previously for Landsat OLI sensor [29], which was applied to and evaluated for only five lakes and was designed to be applicable to images from Landsat OLI. By visually comparing lake ice classification between that using methods from Barbieux *et al.* [29] and SLIDE, we found that while the former can capture dark ice well, it tended to fail when the ice or the snow on the top are optically smooth (Fig. 7). This failure is likely caused by its limited training data.

As suggested by Barbieux *et al.* [29], we confirmed the importance of texture (expressed as the mean gradient of the "Blue" band in our model) on improving classification. Many applications of machine learning to satellite image

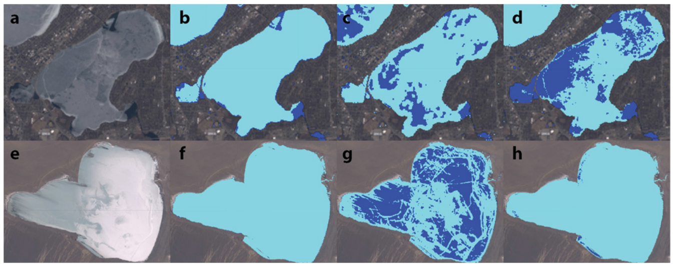

Fig. 7. Comparing snow/ice classification for two example lakes (a) and (e) using the SLIDE model presented in this article (b) and (f), the algorithm by Barbieux *et al.* [29] (c) and (g), and the Fmask (d) and (h). Cyan: snow/ice, blue: water.

classification problems suggest that including texture information can improve accuracy [39]. However, the benefit of this inclusion might be scale dependent. For example, due to changes in resolution of remote sensing images, certain signature textures might be dampened, or entirely lost, with the smoothing effect of coarse resolution. As such, contribution of texture terms might vary when using images with different spatial resolutions, or when applying the algorithm across lakes of various sizes. However, the relative variable importance from our final model (shown in Fig. 4) suggests that images from the Landsat TM, ETM+, and OLI are largely consistent. As a result, the algorithm only requires minor adjustments to be applied across missions.

In situ lake ice phenology provides valuable ground truthing data for developing/evaluating remote sensing algorithms, but challenges still exist for an accurate comparison of these two very different data streams. In our study, to increase the available matchup data between *in situ* and remote sensing for evaluation, we had to assume ice cover fraction based on *in situ* phenological dates. This assumption might not always hold, especially for large lakes whose entire surface can be hard to observe on the ground and for lakes at lower latitudes whose ice cover period can be characterized by multiple freeze-thaw events. While we did not find patterns of latitudinal dependence for model evaluation (Fig. S1), we did notice that remotely sensed ice fraction (from both Fmask and SLIDE) better matches with *in situ* ice cover with decreasing lake size (Fig. S2). Lake ice studies using either *in situ* lake ice data or remote sensing will benefit greatly from having a more explicit documentation of the extent of ice cover, rather than having the dynamic development and melt of lake ice condensed into a few discrete dates (e.g., "ice-on start," "ice-on," and "ice-off"). In addition, with the exciting trend of various citizen science organizations and local government agencies documenting changes in ice cover in lakes [40], [41], it has become even more important to establish a consistent and well-documented protocol to ensure data consistency and quality. For example, including observation viewpoint and exact GPS location would help better spatially match *in situ* and remote sensing datasets. Coordinating the *in situ* data collection with satellite overpasses would also help increase temporally matched data pairs, allowing refining of remote sensing algorithms, which, in return, will help extend observation capacity. Currently, publicly available *in situ* data were clustered in low latitude locations, while the lake-rich high latitude regions lacked sufficient on the ground observations. While this imbalance in *in situ* data availability might bias the model evaluation with *in situ* data toward lakes at lower latitudes, the SLIDE model itself should be less affected, as the training data for the model were collected over both high and low latitude regions (see Fig. 2), regardless of the *in situ* lake ice data availability.

Accurate classification of lake ice using Landsat images allows reconstruction of historical lake ice conditions across the world. Being able to accurately identify lake ice, especially during the transition period, will improve our ability to study ice dynamics and its drivers. Improved ability to detect dark ice will also help more accurately mark the dates of the start of the ice-on and the end of the ice-off. It will improve ice detection for lakes in cold and arid areas (e.g., lakes on the Tibetan Plateau and Central Asia) where dark ice can persist for an extended period of time.

In addition, accurate identification of the presence of ice will help flag the influence of ice in studies that focus on remote sensing of lakes during the open water period. Landsat has been widely tested for its ability to retrieve water quality parameters like clarity [42], [43], chl-a [17], and DOC [20] from lakes. As the applicability of remote sensing-based retrieval algorithms trends toward larger spatial extent [15], it has become more critical to be able to flag those estimated records that are affected by ice cover. As novel datasets (e.g., AquaSat [44]), water quality retrieval algorithms, and lake-focused satellites (e.g., the forthcoming Surface Water and Ocean Topography mission [45]) become available, our proposed method allows more accurate flagging of ice-affected observations.

A comprehensive monitoring of lake ice should use various types of remote sensing sensors by combining their strengths: passive microwave remote sensing for large lakes, optical remote sensing (civilian satellites like Landsat and Sentinel-2 and commercial satellites like those operated by Planet [46]) for lakes with medium and small size, and active microwave remote sensing (e.g., Sentinel-1 and RADARSAT-1/2) for monitoring lakes that are in regions known for inclement weather conditions or in high latitudes. Optical remote sensing is critical in all three approaches as it provides easy-to-interpret visual representation of lake surfaces, extends *in situ* lake ice observation in space and time, provides data for calibration and validation of process-based lake ice models [47], and complements the microwave remote sensing approaches that are mostly limited to larger lakes [48], [49].

Acknowledgment

The authors would like to thank S. Sharma and K. Blagrave for providing the GLRIP dataset with updated lake geolocations and C. D. Arp for providing lake ice phenology for Alaska lakes. They would also like to thank K. Barbieux for providing clarification on their pioneer work designing a lake ice-specific CART model using Landsat.

Code and Data

Training data are available on Zenodo (10.5281/zenodo.4034785). Code used to construct SLIDE, validate, and evaluate model performance will be accessible via GitHub (https://github.com/seanyx/lake-ice-classification). For demonstration of concept, we provided a Google Earth Engine app that can be used to extract multi-temporal lake ice coverage for lakes listed in the HydroLAKES dataset (https://eeproject.users.earthengine.app/view/lake-ice-doy).

References

[1] L. C. Smith, Y. Sheng, and G. M. MacDonald, "A first pan-Arctic assessment of the influence of glaciation, permafrost, topography and peatlands on Northern Hemisphere lake distribution," *Permafrost Periglacial Processes*, vol. 18, no. 2, pp. 201–208, Apr. 2007, doi: 10.1002/ppp.581.

[2] B. A. Denfeld, H. M. Baulch, P. A. D. Giorgio, S. E. Hampton, and J. Karlsson, "A synthesis of carbon dioxide and methane dynamics during the ice-covered period of northern lakes," *Limnol. Oceanogr. Lett.*, vol. 3, no. 3, pp. 117–131, Jun. 2018, doi: 10.1002/lol2.10079.

[3] E. Jeppesen, M. Søndergaard, and J. P. Jensen, "Climatic warming and regime shifts in lake food webs-some comments," *Limnol. Oceanogr.*, vol. 48, no. 3, pp. 1346–1349, May 2003, doi: 10.4319/lo.2003.48.3.1346.

[4] S. M. Powers *et al.*, "Ice duration drives winter nitrate accumulation in north temperate lakes," *Limnol. Oceanogr. Lett.*, vol. 2, no. 5, pp. 177–186, Oct. 2017, doi: 10.1002/lol2.10048.

[5] T. J. Caldwell, S. Chandra, K. Feher, J. B. Simmons, and Z. Hogan, "Ecosystem response to earlier ice break-up date: Climate-driven changes to water temperature, lake-habitat-specific production, and trout habitat and resource use," *Global Change Biol.*, vol. 26, no. 10, pp. 5475–5491, Oct. 2020, doi: 10.1111/gcb.15258.

[6] S. Sharma *et al.*, "Integrating perspectives to understand lake ice dynamics in a changing world," *J. Geophys. Res., Biogeosci.*, vol. 125, no. 8, Aug. 2020, Art. no. e2020JG005799, doi: 10.1029/2020jg005799.

[7] W. Wang *et al.*, "Global lake evaporation accelerated by changes in surface energy allocation in a warmer climate," *Nature Geosci.*, vol. 11, no. 6, pp. 410–414, Jun. 2018, doi: 10.1038/s41561-018-0114-8.

[8] S. E. Hampton *et al.*, "Ecology under lake ice," *Ecol. Lett.*, vol. 20, no. 1, pp. 98–111, Jan. 2017, doi: 10.1111/ele.12699.

[9] K. Salonen, M. Leppäranta, M. Viljanen, and R. D. Gulati, "Perspectives in winter limnology: Closing the annual cycle of freezing lakes," *Aquatic Ecol.*, vol. 43, no. 3, pp. 609–616, Sep. 2009, doi: 10.1007/s10452-009-9278-z.

[10] L. B. Knoll *et al.*, "Consequences of lake and river ice loss on cultural ecosystem services," *Limnol. Oceanogr. Lett.*, vol. 4, no. 5, pp. 119–131, Oct. 2019, doi: 10.1002/lol2.10116.

[11] J. J. Magnuson, "Historical trends in lake and river ice cover in the Northern Hemisphere," *Science*, vol. 289, no. 5485, pp. 1743–1746, Sep. 2000, doi: 10.1126/science.289.5485.1743.

[12] D. F. Schmidt, K. M. Grise, and M. L. Pace, "High-frequency climate oscillations drive ice-off variability for Northern Hemisphere lakes and rivers," *Climatic Change*, vol. 152, nos. 3–4, pp. 517–532, Mar. 2019, doi: 10.1007/s10584-018-2361-5.

[13] B. J. Benson *et al.*, "Extreme events, trends, and variability in Northern Hemisphere lake-ice phenology (1855–2005)," *Climatic Change*, vol. 112, no. 2, pp. 299–323, May 2012, doi: 10.1007/s10584-011-0212-8.

[14] K. Dörnhöfer and N. Oppelt, "Remote sensing for lake research and monitoring—Recent advances," *Ecolog. Indicators*, vol. 64, pp. 105–122, May 2016, doi: 10.1016/j.ecolind.2015.12.009.

[15] S. N. Topp, T. M. Pavelsky, D. Jensen, M. Simard, and M. R. V. Ross, "Research trends in the use of remote sensing for inland water quality science: Moving towards multidisciplinary applications," *Water*, vol. 12, no. 1, p. 169, Jan. 2020, doi: 10.3390/w12010169.

[16] M.-M. Zhang, F. Chen, and B.-S. Tian, "An automated method for glacial lake mapping in High Mountain Asia using Landsat 8 imagery," *J. Mountain Sci.*, vol. 15, no. 1, pp. 13–24, Jan. 2018, doi: 10.1007/s11629-017-4518-5.

[17] E. E. Maeda *et al.*, "Temporal patterns of phytoplankton phenology across high latitude lakes unveiled by long-term time series of satellite data," *Remote Sens. Environ.*, vol. 221, pp. 609–620, Feb. 2019, doi: 10.1016/j.rse.2018.12.006.

[18] D. Liu *et al.*, "Observations of water transparency in China's lakes from space," *Int. J. Appl. Earth Observ. Geoinf.*, vol. 92, Oct. 2020, Art. no. 102187, doi: 10.1016/j.jag.2020.102187.

[19] K. Kallio *et al.*, "Landsat ETM+ images in the estimation of seasonal lake water quality in boreal river basins," *Environ. Manage.*, vol. 42, no. 3, pp. 511–522, Sep. 2008, doi: 10.1007/s00267-008-9146-y.

[20] C. G. Griffin, J. W. McClelland, K. E. Frey, G. Fiske, and R. M. Holmes, "Quantifying CDOM and DOC in major Arctic rivers during ice-free conditions using Landsat TM and ETM+ data," *Remote Sens. Environ.*, vol. 209, pp. 395–409, May 2018, doi: 10.1016/j.rse.2018.02.060.

[21] S. Sharma *et al.*, "Widespread loss of lake ice around the Northern Hemisphere in a warming world," *Nature Climate Change*, vol. 9, no. 3, pp. 227–231, Mar. 2019, doi: 10.1038/s41558-018-0393-5.

[22] B. Benson, J. Magnuson, and S. Sharma, "Global lake and river ice phenology database, version 1," Nat. Snow Ice Data Center, Boulder, CO, USA, 2020. Accessed: Jul. 3, 2020. [Online]. Available: https://nsidc.org/data/G01377/versions/1, doi: 10.7265/N5W66HP8.

[23] M. L. Messager, B. Lehner, G. Grill, I. Nedeva, and O. Schmitt, "Estimating the volume and age of water stored in global lakes using a geo-statistical approach," *Nature Commun.*, vol. 7, no. 1, p. 13603, Dec. 2016, doi: 10.1038/ncomms13603.

[24] T. Šmejkalová, M. E. Edwards, and J. Dash, "Arctic lakes show strong decadal trend in earlier spring ice-out," *Sci. Rep.*, vol. 6, no. 1, pp. 1–8, Dec. 2016, doi: 10.1038/srep38449.

[25] X. Yang, T. M. Pavelsky, and G. H. Allen, "The past and future of global river ice," *Nature*, vol. 577, no. 7788, pp. 69–73, Jan. 2020, doi: 10.1038/s41586-019-1848-1.

[26] N. Chaouch, M. Temimi, P. Romanov, R. Cabrera, G. McKillop, and R. Khanbilvardi, "An automated algorithm for river ice monitoring over the Susquehanna River using the MODIS data," *Hydrol. Processes*, vol. 28, no. 1, pp. 62–73, Jan. 2014, doi: 10.1002/hyp.9548.

[27] S. Zhang and T. M. Pavelsky, "Remote sensing of lake ice phenology across a range of lakes sizes, ME, USA," *Remote Sens.*, vol. 11, no. 14, p. 1718, Jul. 2019, doi: 10.3390/rs11141718.

[28] Z. Zhu, S. Wang, and C. E. Woodcock, "Improvement and expansion of the Fmask algorithm: Cloud, cloud shadow, and snow detection for Landsats 4–7, 8, and Sentinel 2 images," *Remote Sens. Environ.*, vol. 159, pp. 269–277, Mar. 2015, doi: 10.1016/j.rse.2014.12.014.

[29] K. Barbieux, A. Charitsi, and B. Merminod, "Icy lakes extraction and water-ice classification using Landsat 8 OLI multispectral data," *Int. J. Remote Sens.*, vol. 39, no. 11, pp. 3646–3678, Jun. 2018, doi: 10.1080/01431161.2018.1447165.

[30] L. Breiman, "Using iterated bagging to debias regressions," *Mach. Learn.*, vol. 45, no. 3, pp. 261–277, 2001, doi: 10.1023/a:1017934522171.

[31] J.-F. Pekel, A. Cottam, N. Gorelick, and A. S. Belward, "High-resolution mapping of global surface water and its long-term changes," *Nature*, vol. 540, no. 7633, pp. 418–422, Dec. 2016, doi: 10.1038/nature20584.

[32] N. Gorelick, M. Hancher, M. Dixon, S. Ilyushchenko, D. Thau, and R. Moore, "Google Earth engine: Planetary-scale geospatial analysis for everyone," *Remote Sens. Environ.*, vol. 202, pp. 18–27, Dec. 2017, doi: 10.1016/j.rse.2017.06.031.

[33] H. Xu, "Modification of normalised difference water index (NDWI) to enhance open water features in remotely sensed imagery," *Int. J. Remote Sens.*, vol. 27, no. 14, pp. 3025–3033, Jul. 2006, doi: 10.1080/01431160600589179.

[34] A. Hossain, Y. Jia, and X. Chao, "Development of remote sensing based index for estimating/mapping suspended sediment concentration in river and lake environments," in *Proc. 8th Int. Symp. ECOHYDRAULICS (ISE)*, 2010, pp. 578–585. [Online]. Available: https://www.researchgate.net/profile/Akm_Hossain5/publication/251236287_Development_of_Remote_Sensing_Based_Index_for_Estimating_Mapping_Suspended_Sediment_Concentration_in_River_and_Lake_Environments/links/53f34e720cf256ab87b089fe.pdf?inViewer=true&pdfJsDownload=true&disableCoverPage=true&origin=publication_detail

[35] M. L. McHugh, "Interrater reliability: The kappa statistic," *Biochem. Medica*, vol. 22, no. 3, pp. 276–282, 2012, doi: 10.11613/bm.2012.031.

[36] H. Meyer, C. Reudenbach, S. Wöllauer, and T. Nauss, "Importance of spatial predictor variable selection in machine learning applications—Moving from data reproduction to spatial prediction," *Ecol. Model.*, vol. 411, Nov. 2019, Art. no. 108815, doi: 10.1016/j.ecolmodel.2019.108815.

[37] C. D. Arp, B. M. Jones, M. Whitman, A. Larsen, and F. E. Urban, "Lake temperature and ice cover regimes in the Alaskan Subarctic and Arctic: Integrated monitoring, remote sensing, and modeling1," *J. Amer. Water Resour. Assoc.*, vol. 46, no. 4, pp. 777–791, Aug. 2010.

[38] C. D. Arp, B. M. Jones, and G. Grosse, "Recent lake ice-out phenology within and among lake districts of Alaska, U.S.A," *Limnol. Oceanogr.*, vol. 58, no. 6, pp. 2013–2028, Nov. 2013. [Online]. Available: https://aslopubs.onlinelibrary.wiley.com/doi/abs/10.4319/lo.2013.58.6.2013

[39] S. Leigh, Z. Wang, and D. A. Clausi, "Automated ice–water classification using dual polarization SAR satellite imagery," *IEEE Trans. Geosci. Remote Sens.*, vol. 52, no. 9, pp. 5529–5539, Sep. 2014, doi: 10.1109/tgrs.2013.2290231.

[40] G. A. Hodgkins, I. C. James, and T. G. Huntington, "Historical changes in lake ice-out dates as indicators of climate change in New England, 1850–2000," Fact Sheet, U.S. Geolog. Surv., Reston, VA, USA, Tech. Rep. 2005-3002, 2005, doi: 10.3133/fs20053002.

[41] C. P. K. Warne, K. S. McCann, N. Rooney, K. Cazelles, and M. M. Guzzo, "Geography and morphology affect the ice duration dynamics of Northern Hemisphere lakes worldwide," *Geophys. Res. Lett.*, vol. 47, no. 12, Jun. 2020, Art. no. e2020GL087953, doi: 10.1029/2020gl087953.

[42] K. Song *et al.*, "Quantification of lake clarity in China using Landsat OLI imagery data," *Remote Sens. Environ.*, vol. 243, Jun. 2020, Art. no. 111800, doi: 10.1016/j.rse.2020.111800.

[43] S. M. Kloiber, P. L. Brezonik, and M. E. Bauer, "Application of Landsat imagery to regional-scale assessments of lake clarity," *Water Res.*, vol. 36, no. 17, pp. 4330–4340, Oct. 2002, doi: 10.1016/s0043-1354(02)00146-x.

[44] M. R. V. Ross *et al.*, "AquaSat: A data set to enable remote sensing of water quality for inland waters," *Water Resour. Res.*, vol. 55, no. 11, pp. 10012–10025, Nov. 2019, doi: 10.1029/2019wr024883.

[45] S. Biancamaria, D. P. Lettenmaier, and T. M. Pavelsky, "The SWOT mission and its capabilities for land hydrology," in *Remote Sensing and Water Resources*, A. Cazenave, N. Champollion, J. Benveniste, and J. Chen, Eds. Cham, Switzerland: Springer, 2016, pp. 117–147.

[46] S. Cooley, L. Smith, L. Stepan, and J. Mascaro, "Tracking dynamic northern surface water changes with high-frequency planet CubeSat imagery," *Remote Sens.*, vol. 9, no. 12, p. 1306, Dec. 2017, doi: 10.3390/rs9121306.

[47] L. C. Brown and C. R. Duguay, "The response and role of ice cover in lake-climate interactions," *Prog. Phys. Geogr., Earth Environ.*, vol. 34, no. 5, pp. 671–704, Oct. 2010, doi: 10.1177/0309133310375653.

[48] Y. Cai, C.-Q. Ke, and Z. Duan, "Monitoring ice variations in Qinghai Lake from 1979 to 2016 using passive microwave remote sensing data," *Sci. Total Environ.*, vols. 607–608, pp. 120–131, Dec. 2017, doi: 10.1016/j.scitotenv.2017.07.027.

[49] M. Engram, C. D. Arp, B. M. Jones, O. A. Ajadi, and F. J. Meyer, "Analyzing floating and bedfast lake ice regimes across Arctic Alaska using 25 years of space-borne SAR imagery," *Remote Sens. Environ.*, vol. 209, pp. 660–676, May 2018, doi: 10.1016/j.rse.2018.02.022.

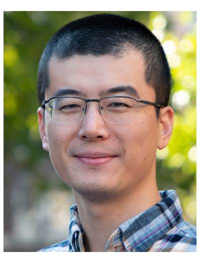

Xiao Yang received the B.S. degree in geophysics from the University of Science and Technology of China, Hefei, China, in 2019, the M.Phil. degree in geophysics from The University of Hong Kong, Hong Kong, in 2012, and the Ph.D. degree in geological sciences from the University of North Carolina at Chapel Hill, Chapel Hill, NC, USA.

He is a Post-Doctoral Research Associate with the Global Hydrology Laboratory, Department of Geological Sciences, University of North Carolina at Chapel Hill. His research focuses on global changes in lakes and rivers and their relationship to climate change.

Tamlin M. Pavelsky received the B.A. degree from the Middlebury College, Middlebury, VT, USA, in 2001, and the M.A. and Ph.D. degrees from the University of California at Los Angeles (UCLA), Los Angeles, CA, USA, in 2004 and 2008, respectively.

He is a Professor with the Department of Geological Sciences, University of North Carolina, Chapel Hill, NC, USA. His research interests focus on global surface water hydrology using a combination of remote sensing, field work, and modeling.

Liam P. Bendezu received the B.A. degree from the University of North Carolina at Chapel Hill, Chapel Hill, NC, USA, in 2021.

He worked as a Research Assistant with the Global Hydrology Laboratory, Department of Geological Sciences, University of North Carolina at Chapel Hill.

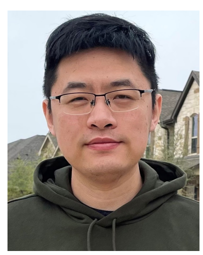

Shuai Zhang received the B.S. degree in surveying from Southeast University, Nanjing, China, in 2008, the M.S. degree in geography information engineering from Wuhan University, Wuhan, China, in 2012, and the Ph.D. degree in civil engineering from Texas A&M University, College Station, TX, USA, in 2017.

He worked as a Post-Doctoral Scholar with the Department of Geological Sciences, University of North Carolina at Chapel Hill, Chapel Hill, NC, USA, from 2017 to 2020. Since 2020, he has been working with the Optical Oceanography Laboratory, College of Marine Science, University of South Florida, Tampa, FL, USA, as a Post-Doctoral Scholar. His research interests include remote sensing of macroalgae blooms, lake ice phenology, and reservoir storage monitoring.